Journal of Solid State Chemistry 182 (2009) 2350–2356

Contents lists available at ScienceDirect

Journal of Solid State Chemistry

journal homepage: www.elsevier.com/locate/jssc

Synthesis and anion exchange properties of a Zn/Ni double hydroxide salt with a guarinoite structure

F. Delorme [a,b,*], A. Seron [a], M. Licheron [c], E. Veron [c], F. Giovannelli [d], C. Beny [a], V. Jean-Prost [a], D. Martineau [a]

[a] BRGM, 3 Avenue Claude Guillemin, BP 36009, 45060 ORLEANS Cedex 2, France
[b] CORNING SAS, CETC, 7 bis Avenue Valvins, 77210 AVON, France
[c] CEMHTI, 1D avenue de la Recherche Scientifique 45071 ORLEANS Cedex 2, France
[d] LEMA, UMR 6157 CNRS-CEA, Université François Rabelais, 3 place Jean Jaurès 41029, BLOIS, France

ARTICLE INFO

Article history:
Received 13 February 2009
Received in revised form
17 April 2009
Accepted 27 May 2009
Available online 2 June 2009

Keywords:
Guarinoite
Hydroxide
Double hydroxide salt
Hydroxyl double salt
Hydroxide double salt

ABSTRACT

In this study, the first route to synthesize a compound with the guarinoite structure $(Zn,Co,Ni)_6(SO_4)(OH,Cl)_{10}\cdot 5H_2O$ is reported. Zn/Ni guarinoite is obtained from the reaction of $NiSO_4\cdot 7H_2O$ with solid ZnO in aqueous solution. The resulting green Zn/Ni guarinoite ($(Zn_{3.52}Ni_{1.63})(SO_4)_{1.33}(OH_{7.64})\cdot 4.67H_2O$) was characterized by X-ray diffraction, infrared spectrometry, UV–Visible spectrometry and thermal analysis. It is shown that its structure is similar to the one described for the layered Zn sulfate hydroxide hydrate, i.e. brucite layers with $\frac{1}{4}$ empty octahedra presenting tetrahedrally coordinated divalent atoms above and below the empty octahedra. Ni atoms are located in the octahedra and zinc atoms in tetrahedra and octahedra. In this structure the exchangeable anions are located at the apex of tetrahedra. Scanning electron microscopy (SEM) and transmission electron microscopy (TEM) observations show that the Zn/Ni guarinoite is composed of aggregates of hexagonal plates of several hundreds of nanometers. Due to its interest for industrial or environmental applications, the exchange of sulfate groups by carbonates has been investigated. Results show a limited exchange and a higher affinity of the Zn/Ni guarinoite for sulfates compared to carbonates.

1. Introduction

Guarinoite ($(ZnCoNi)_6(SO_4)(OH,Cl)_{10}\cdot 5H_2O$) is a mineral that has been discovered in 1993 in the Cap Garonne mine (Var, France). This mine has been worked for copper and lead, but is mostly known to have provided numerous new mineral species such as Perroudite $Hg_5Ag_4S_5(Cl,I,Br)_4$ [1], Geminite $Cu_2As_2O_7\cdot 3H_2O$ [2], Camerolaite $Cu_4Al_2[HSbO_4,SO_4](OH)_{10}(CO_3)\cdot 2H_2O$ [3], Deloryite $Cu_4(UO_2)(MoO_4)_2(OH)_6$ [4], Capgaronite HgS.Ag(Cl,Br,I) [5], Theresemagnanite $(CoZnNi)_6(SO_4)(OH,Cl)_{10}\cdot 8H_2O$ [6], Zdenekite $NaPbCu_5(AsO_4)_4Cl\cdot 5H_2O$ [7], Mahnertite (Na,Ca)-$Cu_3(AsO_4)_2Cl\cdot 4H_2O$ [8], Iltisite HgSAg(Cl,Br) [9], or Pushcharovskite $Cu(AsO_3\cdot OH)\cdot H_2O$ [10].

Sarp [6] has described guarinoite as bright to deep pink aggregates or rounded aggregates made up of thin hexagonal crystals (space group: $P63$, $P63/m$, or $P6322$, with $a = 8.344$ and $c = 21.59$ Å).

Guarinoite is related to the group of hydroxide salts presenting a layered structure. Several different structures are represented in this group. The first one is derived from the structure of brucite $Mg(OH)_2$, where Mg^{2+} cations are occupying the centers of OH^- octahedra joined by their edges to form infinite layers, and where the layers are linked by hydrogen bonds between hydroxyl groups at octahedral vertices. This structure is well represented by the layered double hydroxides (LDHs) family ($[M(II)_{1-x}M(III)_x(OH)_2]\ [A^{n-}]_{x/n}\cdot mH_2O$) where some M^{3+} cations are replacing a part of the M^{2+} cations, thus generating positively charged brucite-like layers that are counterbalanced by anions (A^{n-}) located between the layers [11,12]. These compounds are largely studied as they find many industrial applications such as catalysts, catalyst supports or precursors, anion exchangers, or part of heterostructured nanohybrids [13–16].

The two other structures are represented by basic hydroxides or the double hydroxide salts family (DHS, also known as hydroxyl double salts or hydroxy double salts), in which a part of the divalent cations is not replaced by trivalent cations as in LDHs but is replaced by another divalent cation. The first one is also derived from the structure of brucite, where some OH^- groups are replaced by another anion. The general formula of this family could be written as $(M^{II}_{2-x}M'^{II}_x)(OH)_{2-y}A^{n-}_{y/n}\cdot mH_2O$, where M^{II} and M'^{II} are divalent metal cations such as Zn^{2+}, Cu^{2+}, Co^{2+}, Ni^{2+}, …

* Corresponding author at: Present address: CORNING SAS, CETC, 7 bis Avenue Valvins, 77210 AVON, France. Fax: +33 1 64 69 75 55.
E-mail address: delormef@corning.com (F. Delorme).

0022-4596/$ - see front matter © 2009 Elsevier Inc. All rights reserved.
doi:10.1016/j.jssc.2009.05.031

and A^{n-} an anion such as NO_3^-, Cl^-, SO_4^{2-}, CO_3^{2-}, … [17,18]. Such compounds have been studied, as the anion exchange for large organic species (i.e. aliphatic chain anions) coordinating the metal ion has allowed to tune the interlayer spacing, and thus their magnetic properties [19–23].

The second one is related to the structure of zinc hydroxide nitrate [24,25]. It can be regarded as a variation of a hypothetical $Zn(OH)_2$ structure in the C6 or CdI_2-type group. One quarter of the zinc atoms are removed from the octahedral interstices of the layers. Each filled octahedron shares its edges with two unoccupied and four occupied octahedra. The resulting layer is negatively charged: $[Zn_3^{oct}(OH)_8]^{2-}$. Tetrahedrally coordinated zinc atoms are located above and below the empty octahedron. Three corners of the tetrahedron are occupied by hydroxide ions belonging to the layer described above, the fourth by a water molecule, or another anion [25–27]. Guarinoite and many other Zn/Ni or Zn/Co hydroxide salts belong to this last group.

Most of these compounds have exhibited anion exchange properties [13,17,28–32]. These properties can find many applications. One of the most promising applications is remediation. Indeed many pollutants, from natural or anthropogenic origin, due to high concentrations in water, have disastrous environmental and health implications, such as nitrates [33], fluorides [34] or arsenates [35]. The most studied family of layered hydroxides, i.e. layered double hydroxides, has shown an important limitation for such applications due to their high affinity for carbonates compared to most of the other anions [13]. So, due to the abundance of carbonates in nature, it remains a subject of great interest for environmental applications to find anion exchangers with a low affinity for carbonates.

Many different synthesis routes have been used to obtain these compounds: the most usual synthesis method to obtain such compounds is coprecipitation [12,36], but other routes such as "chimie douce" [37,38] or reaction of a metal salt with a metal oxide or hydroxide [25,28,39–42] have also been used.

As far as the authors know there has been no report on the synthesis of guarinoite in the literature. A few papers have already been published on Zn/Ni hydroxides with different anions [27–29,31,43–47] but none of the synthesized compounds by these authors do present the guarinoite structure.

The aim of this paper is to report a synthesis route for Zn/Ni guarinoite and investigate whether this compound is presenting anion exchange properties.

2. Material and methods

Zn/Ni guarinoite was prepared by a chemical reaction using $NiSO_4 \cdot 7H_2O$ (Prolabo 99%) solution and ZnO powder (Prolabo 99.5%). ZnO powder of 2 g was added to 50 ml of 0.64 M $NiSO_4 \cdot 7H_2O$ aqueous solution (Ni/Zn mole ratio = 1.25) under vigorous stirring at room temperature for 2 h. Then stirring was stopped and the precipitate was aged at room temperature for 1 day. The slurry was centrifuged at 4000 rpm for 5 min (Jouan CR412). The supernatant was eliminated and the sample was dried in a furnace at 40 °C for 24 h.

The anion exchange properties were investigated by mixing 2 g of the synthesized Zn/Ni guarinoite with 100 ml of 0.1 M Na_2CO_3 solution. The mole amount of CO_3^{2-} added was nearly 3 times that of the sulfate content of guarinoite. After equilibrating during 1 day at room temperature, the solid was separated by centrifugation and dried in a furnace at 40 °C for 24 h.

Chemical compositions (Zn and Ni concentrations) have been determined by atomic absorption with a Varian AA 200 after dissolution of the solids by an acid solution composed of HNO_3, HF and $HClO_4$.

Sulfate and carbonate concentrations were determined by measurements of S and C with a Horiba carbon/sulfur analyzer EMIA-820 V.

Powder X-ray diffraction (XRD) patterns have been performed on a Siemens D5000 diffractometer using Co$K\alpha$ radiation operating at 40 kV and 30 mA at room temperature. The scans have been recorded from 4° to 84° (2θ) with a step of 0.02° and a counting time of 1 s per step.

For in-situ temperature study, diffraction data were collected in a conventional Bragg–Brentano configuration with a Vantec-1 linear detector on a X-ray Bruker D8 Advance (Cu$K\alpha_{1,2}$ radiation—40 kV and 40 mA). The diffractometer was equipped with an Anton Paar oven chamber (model HTK1200N) based on a Kanthal® resistive heating attachment for temperature up to 1200 °C. The slits used were 0.3° for the beam and 2.5° Soller for the axial divergence. The diffraction patterns have been recorded between 10° and 70° (2θ) with a step of 0.0164° (2θ). Data acquisition time was 15 min per scan. The heating rate was 10 °C min^{-1} in air and a delay time of 15 min was used to stabilize the sample temperature. Choice of the experimental temperatures was based on the DTA curve to characterize the phenomena observed. The sample temperature has been calibrated using known phase transitions and the thermal expansion of alumina. Peaks have been attributed to the corresponding crystalline phases using ICDD database (PDF-2).

DTA/TG measurements were recorded by a Setaram 92 using platinum crucibles. The powdered samples were analyzed using a heating rate of 10 °C min^{-1} in air (0.5 l h^{-1}).

Infrared spectra were obtained with an attenuated total reflection (ATR) device (Golden Gate) on a Bruker Equinox IFS-55 infrared spectrometer. For each spectrum 20 scans were performed from 4000 to 550 cm^{-1}.

The scanning electron microscopy (SEM) observations have been performed on samples previously sputter-coated with a thin layer of carbon, using a Jeol 6100 coupled with an energy dispersive spectrometer (Kevex Quantum) for chemical analysis, at 25 kV.

The transmission electron microscopy (TEM) observations have been performed at 200 kV (Philips CM20 with a CCD Gatan camera). The TEM samples were prepared by dispersing the powder products in alcohol by ultrasonic treatment, dropping them onto a porous carbon film supported on a copper grid, and then drying them in air.

UV–Visible spectra were obtained on compacted powder sample with an integrating sphere device (Labsphere) on a Perkin Elmer lambda 20 UV–Vis spectrometer. The spectra have been performed in the range of 200–1100 nm with a scan speed of 240 nm min^{-1} at room temperature.

3. Results and discussion

3.1. Structural and thermal characterization

The powder resulting from the synthesis process is a pale green powder. This is far different from the pink color described by Sarp [6] for natural guarinoite. However, this pink color is due to the presence of cobalt ions within the natural guarinoite which are absent from the synthesized compound. Indeed, Zn/Ni double hydroxide salts were described as green powders [27,28,31,44,45] and pale green films [29].

Fig. 1a shows the X-ray diffraction pattern of the synthesized green powder. The diffraction peaks correspond to that of the hexagonal guarinoite mineral with the chemical formula $(Zn,Co,Ni)_6(SO_4)(OH,Cl)_{10} \cdot 5H_2O$ (JCPDS 46-1276). Indexed peaks

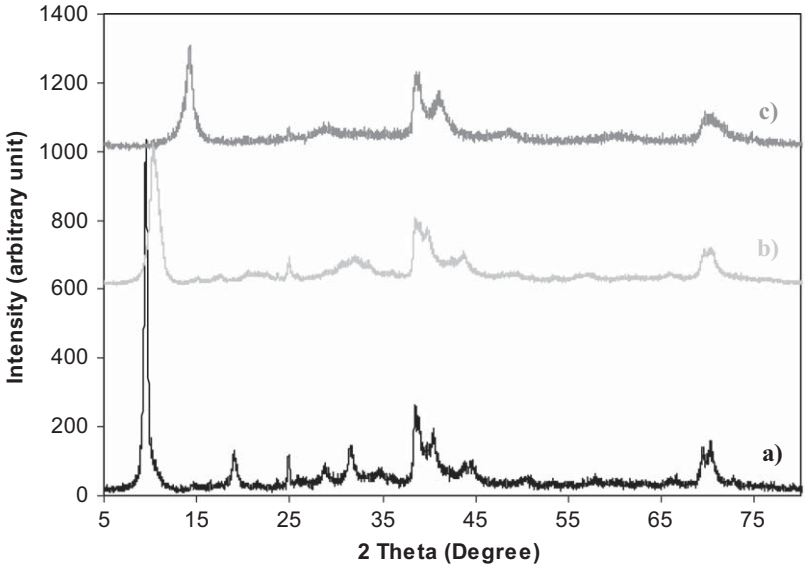

Fig. 1. PXRD patterns of (a) synthesized Zn/Ni guarinoite, (b) long-term X-ray irradiated guarinoite, (c) the carbonate-exchanged Zn/Ni guarinoite.

Table 1
Comparison of X-ray powder diffraction data for the synthesized Zn/Ni guarinoite material and guarinoite mineral JCPDS 46-1276.

h k l	Guarinoite mineral (JCPDS 46-1276)		Synthesized Zn/Ni guarinoite	
	d (Å)	*I*	*d* (Å)	*I*
0 0 2	10.800	100	10.779	100
1 0 0	7.210	5	7.016	4
0 0 4	5.400	25	5.419	13
1 1 0	4.166	20	4.151	11
1 1 2	3.888	5	–	–
2 0 0	3.613	10	3.604	9
1 1 3	3.613			
0 0 6	3.597	5	–	–
1 1 4	3.300	90	3.292	13
			3.283	14
2 0 4	2.986	10	3.012	8
1 1 5	2.986			
1 2 0	2.725	60	2.714	26
1 1 6	2.725			
1 2 1	2.700	5	2.694	22
0 0 8	2.700			
1 2 3	2.563	50	2.589	18
3 0 0	2.407	5	–	–
3 0 1	2.407			
3 0 2	2.351	40	2.353	20
2 0 7	2.351			
2 2 0	2.083	10	2.095	6
3 0 6	2.001	5	1.995	5
2 0 1 0	1.853	10	–	–
4 0 2	1.781	10	–	–
2 2 9	1.575	30	1.570	14
4 1 2	1.560	25	1.567	11
4 0 7	1.560		1.555	14

of the synthesized and mineral guarinoite are included in Table 1. This table shows that the peaks of the synthesized green powder are similar to those of the natural guarinoite mineral, and that all the peaks of the X-ray diffraction pattern are related to the guarinoite. This means that no other phase is present in the sample, and in particular no precursor. The absence of solid ZnO implies that the totality of the ZnO powder has reacted during the synthesis process.

A long-term exposition to the X-ray irradiation has been performed in order to obtain data suitable for Rietveld refinement. However, this irradiation leads to a decrease in crystallinity, and a decrease of the *c*-parameter (Fig. 1b). A similar behavior has been reported for other Zn/Ni hydroxy sulfates when drying at 100 or 110 °C [28,43].

The chemical analysis shows that the compound is only composed by Zn, Ni, S, O, and H (Table 2). The chemical formula, calculated from the metal ion contents, S content, and the water content determined from the weight loss by heating at 250 °C, is given in Table 2. The hydroxide content was calculated on the basis of the condition of electrical neutrality. The Ni/Zn molar ratio of the starting reaction solution was 1.25, and the ratio of the synthesized guarinoite obtained by chemical analysis is 0.46. As no solid ZnO is remaining in the synthesized sample, the variation of the Ni/Zn ratio means that an excess of Ni and SO_4^{2-} remains in the solution eliminated by centrifugation. With the exception of cobalt, the composition of the synthesized guarinoite ($(Zn_{3.52}Ni_{1.63})(SO_4)_{1.33}(OH)_{7.64} \cdot 4.67H_2O$) is close to that observed for the mineral guarinoite [6].

Fig. 2a shows the infrared spectrum of the synthesized Zn/Ni guarinoite. The large peak between 3700 and 2600 cm^{-1} is corresponding to the OH vibrations in hydroxyl groups and water. This peak is very large as the vibrating OH groups can belong to hydroxyl or water, that some can be hydrogen bonded or not, and that in the brucite-like layer, several kinds of hydroxyl groups exist as they can be $Zn_3(OH)$, $Ni_3(OH)$, $Zn_2Ni(OH)$, $ZnNi_2(OH)$, …. The presence of water is confirmed by the peak at 1620 cm^{-1} corresponding to the bending of OH in water. The peak at 941 cm^{-1} can be assigned to Zn or Ni in octahedral environment δ MOH bending vibrations. As Zn–O and Ni–O vibrations, in tetrahedral or octahedral environment, are expected at low wavenumbers, absorption peaks at 1162 (sh), 1112, 1051 (sh), 1015, 660 and 588 cm^{-1} have to be attributed to the vibrations of the SO_4^{2-} groups. These values are different from that of the vibrations of the uncoordinated SO_4^{2-} groups in the T_d point group ($\nu_1 = 983\ cm^{-1}$, $\nu_2 = 450\ cm^{-1}$, $\nu_3 = 1105\ cm^{-1}$ and $\nu_4 = 611\ cm^{-1}$) [48,49]. The symmetric stretching ν_1 is nondegenerate, the bending ν_2 is doubly degenerate, and the asymmetric stretching ν_3 and the second bending ν_4 are triply degenerate. Only the ν_3 and ν_4 are infrared active. In the case of a monodentate sulfate, the symmetry is lowered to C_{3v}, leading to the apparition of the ν_1 band around 975 cm^{-1} and the splitting of the ν_3 band into two peaks. In the case of a bidentate sulfate, the

Table 2
Chemical analysis and lattice parameters of the synthesized Zn/Ni guarinoite.

	Mineral guarinoite		Synthesized guarinoite	
Lattice parameter (nm)	$a = 0.8344$		$a = 0.8323$	
	$c = 2.159$		$c = 2.156$	
Weight (%)	ZnO	33.31	ZnO	42.07
	CoO	22.17	CoO	–
	NiO	6.74	NiO	17.82
	CuO	0.05	CuO	–
	SO_3	11.85	SO_3	15.61
	Cl	0.77	Cl	–
	H_2O	24.4	H_2O	22.80
Chemical formula	$(Zn_{2.99}Co_{2.16}Ni_{0.66})(SO_4)_{1.08}(OH_{9.30}Cl_{0.16}) \cdot 5.23H_2O$		$(Zn_{3.52}Ni_{1.63})(SO_4)_{1.33}(OH_{7.64}) \cdot 4.67H_2O$	

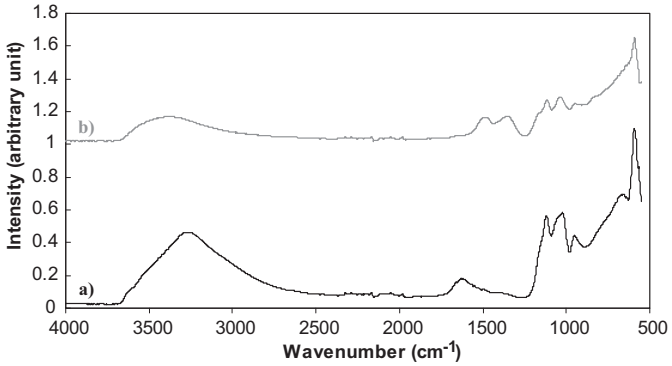

Fig. 2. ATR-FTIR spectrum of (a) the synthesized Zn/Ni guarinoite, (b) the carbonate-exchanged Zn/Ni guarinoite.

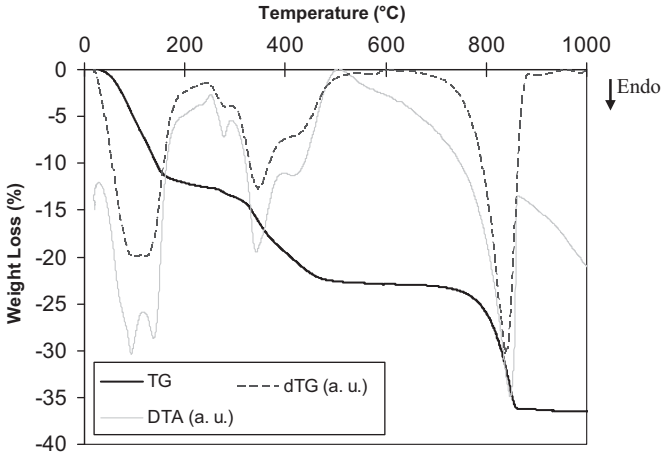

Fig. 3. DTA/TG curves of the synthesized Zn/Ni guarinoite.

symmetry is lowered to C_{2v}, leading to the apparition of the v_1 band but also to the splitting of the v_3 band into three peaks. The three peaks in Zn/Ni guarinoite at 1162, 1112, and 1051 cm^{-1} can be assigned to the splitting of the v_3 band, and the peak at 1015 cm^{-1} to the v_1 band. This means that the sulfate groups in Zn/Ni guarinoite are bidentate. Moreover, as these bands do not show a shift to higher wavenumbers, it can be inferred that the sulfate groups are connected to two atoms (bidentate binuclear), probably the metal atoms of the tetrahedra, or one metal atom of the tetrahedra and one proton, or two protons. The peaks at 660 and 588 cm^{-1} correspond to v_4 vibrations of the sulfate groups.

Fig. 3 shows that all the DTA endothermic peaks are correlated to the dTG peaks, i.e. that all the reactions are connected to weight variations. Upon heating, Zn/Ni guarinoite exhibits three weight losses. The first step between room temperature and 250 °C shows a weight loss of approximately 12.6%. Two endothermic DTA peaks are correlated to this weight loss and have to be related to the loss of surface and interlayer water. A weight loss of 12.6% corresponds to about 4.67 H_2O molecules. A second step, between 250 and 550 °C, shows a weight loss of approximately 10.2%. Three endothermic DTA peaks are correlated to this weight loss and have to be related to the dehydroxylation of the structure. Finally, a third step is observed between 650 and 900 °C, showing a weight loss of approximately 13.4%. This weight loss has to be related to the decomposition of sulfate groups. These values are consistent with those that can be obtained from the calculated chemical composition. The H_2O content has been estimated from the weight loss at 250 °C. According to the calculated chemical composition, the loss of the hydroxyl groups would lead to a weight loss of 10.3% and the loss of the sulfate groups to a weight loss of 15%. These values are consistent with the observed weight losses. Moreover, this interpretation of the thermal data is in accordance with those presented in the literature for sulfate-LDHs [50], Ni basic sulfate [51] and SO_4^{2-}-exchanged Ni–Zn hydroxy acetates [31].

SEM observations (Fig. 4a) show that the synthesized Zn/Ni guarinoite is composed of aggregates from several micrometers to several tenths of micrometers. Higher magnification observations (Fig. 4b) and TEM observations (Fig. 4c and d) show that these aggregates are composed of small plate-like particles from $\frac{1}{2}$ μm to less than 100 nm highly imbricate. This sand-rose morphology is very common for precipitated hydroxides [52–54].

The main difference of the Zn/Ni guarinoite compared to other Zn–Ni DHS already reported lies in the presence of the sulfate groups and in the Ni/Zn ratio. Indeed, the synthesized Zn/Ni guarinoite exhibits a Ni/Zn ratio of 0.46. Except for Stählin and Oswald [27] where Ni/Zn = 0.17, the DHS synthesized by other authors were richer in Ni from 0.56 [28] to 2.44 [43]. Moreover, from the precipitation of Ni and Zn sulfates, Tessier et al. [46] have shown that a pure Ni/Zn phase exists for 35% Zn content, and not for 50% Zn. The nature of the metal atoms in the tetrahedra (Ni or Zn) is debated. Indeed, according to Stählin and Oswald [27], Ni atoms are mainly tetrahedrally coordinated, whereas according to Choy et al. [45], from XANES experiments, Ni atoms are in octahedral sites and Zn atoms in tetrahedral sites. This apparent discrepancy could be related to the difference in Ni/Zn ratios, 0.17 [27] and between 1.42 and 2.27 [45]. Concerning, the synthesized Zn/Ni guarinoite, the UV–Visible spectrum (Fig. 5) mainly shows 4 large bands at 381, 655 and more than 1100 nm. Absorption bands of Ni^{2+} in octahedral environment have been reported corresponding to transition $^3A_{2g} \rightarrow {}^3T_{2g}$ (F) at 1150 nm, $^3A_{2g} \rightarrow {}^3T_{1g}$ (F) at 650 nm and

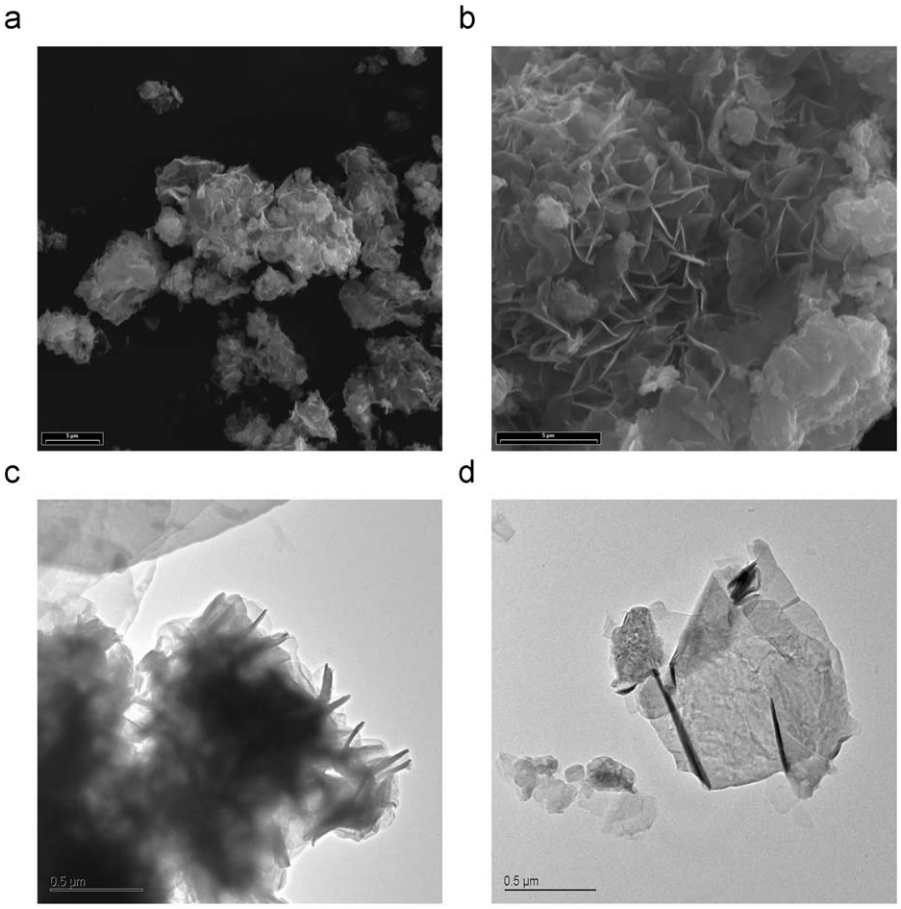

Fig. 4. (a) SEM micrograph (secondary electrons) of aggregates of the synthesized Zn/Ni guarinoite, (b) SEM micrograph (secondary electrons) of the synthesized Zn/Ni guarinoite showing that aggregates are composed by small plate-like particles, (c) TEM micrograph (bright field) of the synthesized Zn/Ni guarinoite showing aggregates, (d) TEM micrograph (bright field) of the synthesized Zn/Ni guarinoite showing isolated plate-like particles.

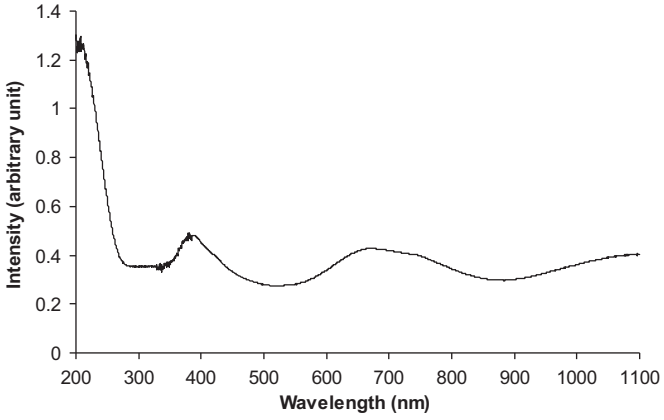

Fig. 5. UV–Vis spectrum of the synthesized Zn/Ni guarinoite.

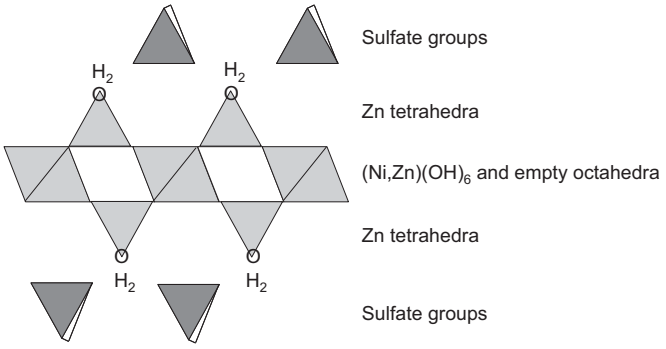

Fig. 6. Schematic representation of the structure of guarinoite.

$^3A_{2g} \rightarrow {}^3T_{1g}$ (P) at 390 nm [55,56]. This confirms that Ni atoms are in octahedra, and thus that tetrahedra should be occupied by Zn atoms. However, due to the high Zn concentration in the Zn/Ni guarinoite, some octahedra have to be occupied by Zn atoms.

Finally, the *c*-parameter decreases when heating at temperatures close to 100 °C, or when exposed to long time X-ray irradiation has to be related with a loss of water. The contraction of the structure along the *c*-direction surely means that the bidentate binuclear sulfate groups are connected at least to one molecule of water, rather than directly connected to tetrahedrally coordinated Zn atoms (Fig. 6).

3.2. Thermal-dependent structure evolution/characterization

HT XRD experiments have been performed to obtain information about the degradation of Zn/Ni guarinoite. Fig. 7 shows the diffraction patterns evolution during heat treatment from 30 to 1100 °C.

Main peaks (d_{002}, d_{004}) of the synthesized Zn/Ni guarinoite disappear when temperature rises by 100 °C. Indeed the material loses interlayer water, inducing decrease of the interlayer distance. At 150 °C all the interlayer water has been lost and the material crystallizes in the $(Zn,Ni)_4SO_4(OH)_6 \cdot 0.5H_2O$ structure which is the only one observed up to 250 °C. Attention must be drawn to the fact that diffraction

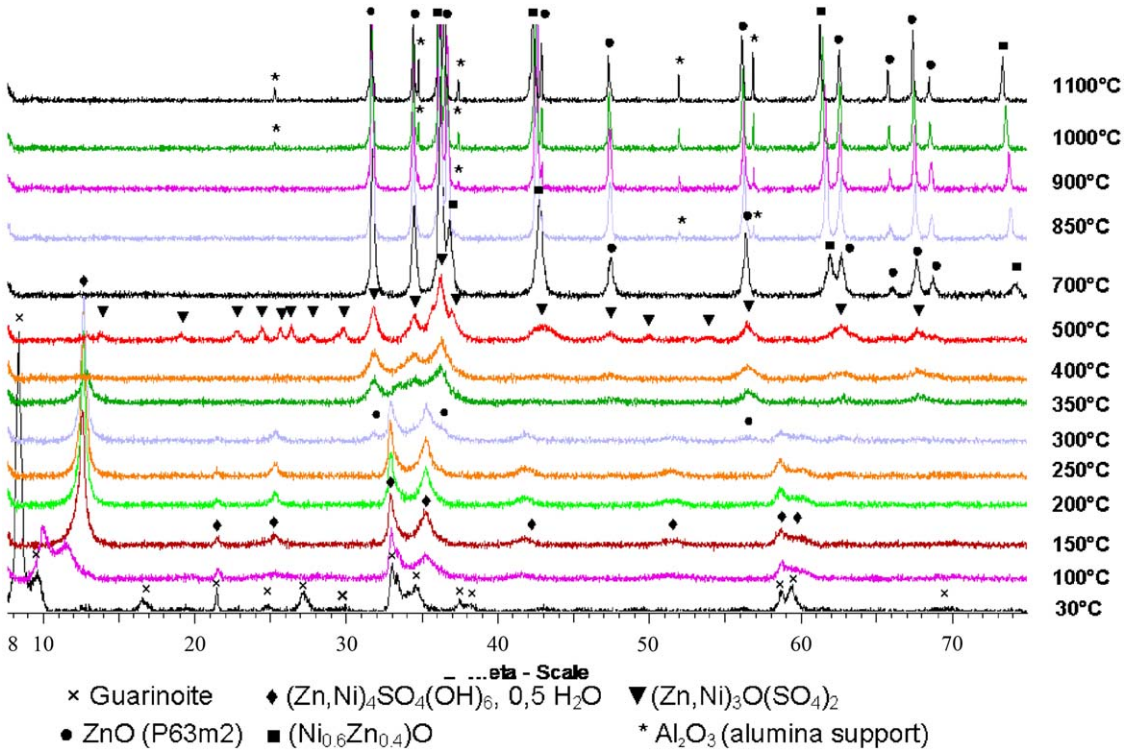

Fig. 7. HT XRD patterns at 30, 100, 150, 200, 250, 300, 350, 400, 500, 700, 850, 900, 1000 and 1100 °C.

lines can be shifted by temperature increase. Around 300 °C, the first diffraction lines of zinc oxide (*P*63*m*2) (JCPDS 76-0704) is detected and the decomposition of $(Zn,Ni)_4SO_4(OH)_6 \cdot 0.5H_2O$ appears as a progressive phenomena. The decomposition of $(Zn,Ni)_4SO_4(OH)_6 \cdot 0.5H_2O$ is complete at 450 °C. After heating up to 500 °C, Zn/Ni guarinoite is decomposed in $(Zn,Ni)_3O(SO_4)_2$. At 700 °C the main peaks of the $(Ni_{0.6}Zn_{0.4})O$ cubic phase (JCPDS 75-0273) are present. Above 900 °C the solid is a mixture of hexagonal ZnO (*P*63*mc*), and cubic $(Ni_{0.6}Zn_{0.4})O$. Diffraction lines of corundum Al_2O_3 are observed too. Indeed when the compound is sintered, its volume is reduced and a part of the alumina support interacts with X-rays. Up to 1100 °C, only the crystallinity of the powder is improved.

In-situ HT XRD brings complementary informations which can be correlated with DTA/TG data. The endothermic peaks around 93 and 140 °C are due to the release of the interlayer water which is obtained in two steps as shown by HT XRD. Between 150 and 250 °C no thermal event is observed on the DTA/TG curves and the XRD patterns are unchanged. The small endothermic peak around 280 °C is due to the destruction of a part of the hydroxide as confirmed by the appearance of the first XRD lines of zinc oxide. Total decomposition of $(Zn,Ni)_4SO_4(OH)_6 \cdot 0.5H_2O$ is observed only after the end of the second weight loss. The decomposition of the sulfate $(Zn,Ni)_3O(SO_4)_2$ with the dissipation of SO_3 gas, similar to that observed for ktenasite [42] corresponds with the last endothermic peak at 848 °C.

3.3. Exchange properties

The PXRD pattern of the carbonate-exchanged Zn/Ni guarinoite is shown in Fig. 1c. Intercalation of CO_3^{2-} in the Zn/Ni guarinoite results in a decrease of the interlayer space with a decrease in basal spacing from 21.56 to 14.47 Å. Moreover, the full width at half maximum of the (002) peak is increased from 0.400° to 0.878° (2θ). This implies a lower crystallinity, and more peculiarly a less ordered structure along the *c*-axis. Other peaks whose basal contribution is absent (like 1 0 0, 1 1 0, …) do not seem significantly affected, signifying that the general structure of the compound is maintained, and that the disorder generated by the carbonate exchange is mainly located along the *c*-axis.

The chemical analysis confirms the presence of carbonate in the sample, but also that sulfur is still present. Indeed, the sulfur concentration is only divided by two. This means that the exchange was not total and that only half of the sulfate groups have been exchanged with carbonate groups.

Fig. 2b presents the infrared spectrum of the carbonate-exchanged Zn/Ni guarinoite. The peaks at 1162 (sh), 1112, 1051 (sh), 1015, 660 and 588 cm^{-1} corresponding to the sulfate groups are still present even if their intensity is lower compared to the as-grown guarinoite. This is consistent with the chemical analysis showing that only half of the sulfate groups have been exchanged. Moreover, the intensity of the peaks related to water is also lowered and the peak at 1620 cm^{-1} has nearly disappeared. However the main difference between infrared spectra of the Zn/Ni guarinoite before and after carbonate exchange is the appearance of two peaks at 1463 and 1336 cm^{-1}. The free CO_3^{2-} ion has D_{3h} symmetry (trigonal planar) and the main infrared active band is the ν_3 band (asymmetric stretching) near 1390 cm^{-1}. The lowering of the symmetry from D_{3h} to C_{2v} leads to the apparition of the ν_1 band around 1068 cm^{-1} and the splitting of the ν_3 band into two peaks. The degree of splitting ($\Delta\nu_3$) allows to make the distinction between monodentate species ($\Delta\nu_3 = 80$–$140\ cm^{-1}$), bidentate binuclear species ($\Delta\nu_3 = 310$–$340\ cm^{-1}$) and bridging bidentate species ($\Delta\nu_3 = 400$–$750\ cm^{-1}$) [57–59]. The synthesized Zn/Ni guarinoite presents a $\Delta\nu_3$ of 127 cm^{-1}. This indicates that the exchanged carbonate groups are monodentate species whereas sulfate groups are still bidentate.

This change in anion group bonding, and the planar nature of the carbonate anion compared to the 3-D nature of the sulfate group, is consistent with the decrease of the *c*-parameter observed after carbonate exchange.

This higher affinity for sulfate anions compared to carbonate anions is of great interest. Indeed, the more studied LDH compounds show a very strong affinity for carbonates [13], that restricts their utilization for environmental applications, due to the ubiquity of carbonates in environment. Zn/Ni guarinoite could thus find many applications as anion trap for environmental purposes.

4. Conclusion

In this study, the first route to synthesize Zn/Ni guarinoite is reported. The resulting Zn/Ni green compound shows that its structure is similar to the one described for the layered zinc sulfate hydroxide hydrate, i.e. brucite layers with $\frac{1}{4}$ empty octahedra presenting tetrahedrally coordinated divalent atoms above and below the empty octahedra. UV–Visible spectrum is showing that Ni atoms are located in the octahedra and zinc atoms in tetrahedra and octahedra. In this structure the exchangeable anions are located at the apex of tetrahedra. Infrared study demonstrates that the sulfate groups are bidentate binuclear, i.e. are connected to two atoms. The *c*-parameter decrease, when heating at temperatures close to 100 °C, or when exposed to long time X-ray irradiation, has to be related with a loss of water. The contraction of the structure along the *c*-direction surely means that the bidentate binuclear sulfate groups are connected at least to one molecule of water, rather than directly connected to tetrahedrally coordinated Zn atoms. SEM and TEM observations show that the Zn/Ni guarinoite is composed by aggregates of hexagonal plates of several hundreds of nanometers.

The synthesized Zn/Ni guarinoite has shown anion exchange properties. However, in the experimental conditions chosen (nearly 3 times the amount of CO_3^{2-} anions compared to the sulfate content of guarinoite), the exchange of carbonates for sulfates is not total, indicating that the affinity for sulfates is stronger than the affinity for carbonates. This is a very different behavior compared to LDHs, where the affinity for carbonate is very strong. These first results are very promising for environmental applications and an extensive detailed study of the affinity of Zn/Ni guarinoite for various anionic pollutants, both organic and inorganic is required.

Acknowledgment

The authors would like to thank D. Jalabert (University of Orleans) for technical support for the TEM observations.

References

[1] H. Sarp, W.D. Birch, P.F. Hlava, A. Pring, D.K.B. Sewell, E.H. Nickel, Am. Mineral. 72 (1987) 1251–1262.
[2] H. Sarp, P. Perroud, Schweiz. Mineral. 70 (1990) 309–314.
[3] H. Sarp, P. Perroud, Neues Jahrbuch für Mineralogie - Monatshefte 11 (1991) 481–486.
[4] H. Sarp, P.J. Chiappero, Neues Jahrbuch für Mineralogie - Monatshefte 2 (1992) 58–64.
[5] B. Mason, W.G. Mumme, H. Sarp, Am. Mineral. 77 (1992) 197–200.
[6] H. Sarp, Archs. Sci. Genève 46 (1993) 37–44.
[7] P.J. Chiappero, H. Sarp, Eur. J. Mineral. 7 (1995) 553–557.
[8] H. Sarp, Archs. Sci. Genève 49 (1996) 119–124.
[9] H. Sarp, J. Sanz-Gysler, P. Perroud, Archs. Sci. Genève 50 (1997) 1–5.
[10] H. Sarp, J. Sanz-Gysler, Archs. Sci. Genève 50 (1997) 177–186.
[11] W.T. Reichle, Solid State Ionics 22 (1986) 135–141.
[12] F. Cavani, F. Trifiro, A. Vaccari, Catal. Today 11 (1991) 173–301.
[13] S. Miyata, Clays Clay Miner. 31 (1983) 305–311.
[14] W. Kagunya, Z. Hassan, W. Jones, Inorg. Chem. 35 (1996) 5970–5974.
[15] A. Vaccari, Catal. Today 41 (1998) 53–71.
[16] J.-H. Choy, J. Phys. Chem. Solids 65 (2004) 373–383.
[17] M. Meyn, K. Beneke, G. Lagaly, Inorg. Chem. 29 (1990) 5201–5207.
[18] H. Morioka, H. Tagaya, M. Karasu, J.-I. Kadokawa, K. Chiba, J. Mater. Res. 13 (1998) 848–851.
[19] P. Rabu, S. Angelov, P. Legoll, M. Belaiche, M. Drillon, Inorg. Chem. 32 (1993) 2463–2468.
[20] W. Fujita, K. Awaga, Inorg. Chem. 35 (1996) 1915–1917.
[21] V. Laget, S. Rouba, P. Rabu, C. Hornick, M. Drillon, J. Magn. Magn. Mater. 154 (1996) L7–L11.
[22] V. Laget, C. Hornick, P. Rabu, M. Drillon, J. Mater. Chem. 9 (1999) 169–174.
[23] P. Rabu, M. Drillon, C. Hornick, Analusis 28 (2000) 103–108.
[24] W. Nowacki, J.N. Silverman, Z. Kristallogr. 115 (1961) 21–51.
[25] W. Stählin, H.R. Oswald, Acta Cryst. B 26 (1970) 860–863.
[26] W. Stählin, H.R. Oswald, J. Solid State Chem. 3 (1971) 252–255.
[27] W. Stählin, H.R. Oswald, J. Solid State Chem. 3 (1971) 256–264.
[28] M. Meyn, K. Beneke, G. Lagaly, Inorg. Chem. 32 (1993) 1209–1215.
[29] H. Nishizawa, K. Yuasa, J. Solid State Chem. 141 (1998) 229–234.
[30] S.P. Newman, W. Jones, J. Solid State Sci. 148 (1999) 26–40.
[31] R. Rojas, C. Barriga, M.A. Ulibarri, P. Malet, V. Rives, J. Mater. Chem. 12 (2002) 1071–1078.
[32] G.G.C. Arizaga, K.G. Satyanarayana, F. Wypych, Solid State Ionics 178 (2007) 1143–1162.
[33] D. Widory, W. Kloppmann, L. Chery, J. Bonnin, H. Rochdi, J.-L. Guinamant, J. Contaminant Hydrol. 72 (2004) 165–188.
[34] H. Mjengera, G. Mkongo, Phys. Chem. Earth 28 (2003) 1097–1104.
[35] M.A. Hossain, Reg. Dev. Dialogue 23 (2002) 83–108.
[36] S. Miyata, T. Kumura, Chem. Lett. (1973) 843–848.
[37] M. Taibi, S. Ammar, N. Jouini, F. Fievet, P. Molinie, M. Drillon, J. Mater. Sci. 12 (2002) 3238–3244.
[38] M. Taibi, S. Ammar, N. Jouini, F. Fievet, J. Phys. Chem. Solids 67 (2006) 932–937.
[39] A. Recoura, C. R. Hebd. Seances Acad. Sci. 132 (1901) 1414–1416.
[40] P. Sabatier, C. R. Hebd. Seances Acad. Sci. 132 (1901) 1538–1540.
[41] H.-P. Boehm, J. Steinle, C. Vieweger, Angew. Chem. Int. Ed. Engl. 16 (1977) 265–266.
[42] M. Xue, R. Chitrakar, K. Sakane, K. Ooi, S. Kobayashi, M. Ohnishi, A. Doi, J. Solid State Chem. 177 (2004) 1624–1630.
[43] S. Yamanaka, K. Ando, M. Ohashi, Mater. Res. Soc. Symp. Proc. 371 (1995) 131–142.
[44] J.-H. Choy, Y.-M. Kwon, S.-W. Song, S.H. Chang, Bull. Korean Chem. Soc. 18 (1997) 450–453.
[45] J.-H. Choy, Y.-M. Kwon, K.-S. Han, S.-W. Song, S.H. Chang, Mater. Lett. 34 (1998) 356–363.
[46] C. Tessier, L. Guerlou-Demourgues, C. Faure, A. Demourgues, C. Delmas, J. Mater. Chem. 10 (2000) 1185–1193.
[47] J. Arulraj, J.T. Rajamathi, R.P. Kandikere, M. Rajamathi, Solid State Sci. 9 (2007) 812–816.
[48] P. Persson, L. Lövgren, Geochim. Cosmochim. Acta 60 (1996) 2789–2799.
[49] D. Peak, R.G. Ford, D.L. Sparks, J. Colloid Interface Sci. 218 (1999) 289–299.
[50] R.L. Frost, M.L. Weier, M.E. Clissold, P.A. Williams, J.T. Kloprogge, Thermochim. Acta 407 (2003) 1–9.
[51] M. Ocaña, J. Colloid Interface Sci. 228 (2000) 259–262.
[52] S. Miyata, Clays Clay Miner. 28 (1980) 50–56.
[53] M. Adachi-Pagano, C. Forano, J.-P. Besse, J. Mater. Chem. 13 (2003) 1988–1993.
[54] E. Geraud, V. Prevot, F. Leroux, J. Phys. Chem. Solids 67 (2006) 903–908.
[55] A. Von Ludi, W. Feitknecht, Hel. Chim. Acta 248 (1963) 2226–2238.
[56] C. Faure, C. Delmas, M. Fouassier, P. Willmann, J. Power Sources 35 (1991) 249–261.
[57] C. Su, D.L. Suarez, Clays Clay Miner. 45 (1997) 814–825.
[58] H. Wijnja, C.P. Schulthess, Soil Sci. Soc. Am. J. 65 (2001) 324–330.
[59] M. Villalobos, J.O. Leckie, J. Colloid Interface Sci. 235 (2001) 15–32.